

Bypass mechanism of F₁-ATPase for asymmetric enzyme kinetics

Yohei Nakayama and Shoichi Toyabe*

*Department of Applied Physics, Graduate School of Engineering,
Tohoku University, Aoba 6-6-05, Sendai 980-8579, Japan*

(Dated: February 28, 2024)

We discovered novel enzyme kinetics of F₁-ATPase, a biomolecular motor that synthesizes and hydrolyzes adenosine triphosphate (ATP), using single-molecule experiments and numerical simulations. The enzyme kinetics of F₁-ATPase followed the Michaelis-Menten equation in ATP hydrolysis but deviated from it in ATP synthesis, indicating asymmetric enzyme kinetics between ATP synthesis and hydrolysis. Numerical analysis based on a theoretical model revealed a bypass mechanism underlying asymmetric enzyme kinetics. In particular, we found that the origin of the asymmetric enzyme kinetics lies in the asymmetry of the allostereism, not in the asymmetry of potential shapes. The asymmetric enzyme kinetics may suggest that F₁-ATPase is designed to sustain the rate of ATP synthesis while suppressing the futile ATP consumption.

Enzymes are catalysts that maintain biological activity by regulating the rates of various reactions in vivo. One of the most important and basic characteristics of enzymes is enzyme kinetics [1], that is, the dependence of reaction rate V on substrate concentration $[S]$. The Michaelis-Menten equation

$$V = \frac{V_{\max}[S]}{K_m + [S]} \quad (1)$$

plays a fundamental role in enzyme kinetics. Because various enzymatic reactions follow Eq. (1), the maximum rate V_{\max} and Michaelis constant K_m are used to characterize these reactions. In addition, deviations from Eq. (1) suggest that the enzyme activity is regulated, for example, by the cooperativity of multiple binding sites.

Enzyme kinetics have been used to investigate the mechanisms underlying a molecular motor F₁-ATPase (F₁). F₁ is an enzyme that synthesizes adenosine triphosphate (ATP), which is also referred to as the “currency of energy in cells,” in aerobic respiration and photosynthesis and plays an essential role in energy metabolism. F₁ has three catalytic sites located at three interfaces between α and β subunits, which consist of the $\alpha_3\beta_3$ ring surrounding the γ subunit [2]. The deviation in the enzyme kinetics of F₁ from those of Eq. (1) [3] was originally examined in the context of the cooperativity of three catalytic sites [4–9], and was later revealed to be caused by the regulatory effect of non-catalytic sites [10].

In this Letter, we focus on the asymmetry of the enzyme kinetics of F₁ between ATP synthesis and hydrolysis. In vivo, F₁ is driven by another molecular motor F_o which applies an external torque to F₁, whereas F₁ catalyses ATP hydrolysis when the external torque is absent or small. In this sense, F₁ is reversible. However, F₁ employs mechanisms to asymmetrically regulate the enzymatic activity between ATP synthesis and hydrolysis, such as ADP-inhibition, ϵ subunit, and regulatory protein IF₁ [11]. Since these mechanisms pause the enzyme activity under conditions that promote ATP hydrolysis, it may be considered that F₁ is designed to sustain the

rate of ATP synthesis while suppressing the futile consumption of ATP synthesized by itself. Recently, in addition to these mechanisms, it has been theoretically implied that the allosteric interaction between the rotary shaft and the binding sites is itself asymmetric between ATP synthesis and hydrolysis [12, 13]. The asymmetric allostereism should result in asymmetric enzyme kinetics. We investigated the asymmetry in the enzyme kinetics of F₁ in single-molecule experiments and numerical simulations to verify the asymmetric allostereism.

Experiments.— We observed the rotation of F₁ in single-molecule experiments with an electrorotation method [14, 15]. The experimental setup is basically the same as that in [16] (See the Supplemental Material [17] for details). Briefly, the rotation of a single F₁ molecule fixed on a Ni-NTA-modified coverslip was observed with a microscope by attaching a probe particle to its rotary shaft (γ subunit). Since F₁ hydrolyzes ATP and rotates its rotary shaft counterclockwise when viewed from the protruded rotary shaft in the absence of external torque N_{ex} [18], we applied the external torque by using electro-rotation method instead of F_o motor in order to observe the clockwise rotation of F₁ [19]. In the clockwise rotation, it was confirmed that F₁ synthesizes ATP [20, 21]. The experiments were performed at room temperature ($25 \pm 1^\circ\text{C}$).

In order to examine the enzyme kinetics, the reaction rate should be measured as a function of the substrate concentration. However, the substrates of ATP synthesis, adenosine diphosphate (ADP) and inorganic phosphate (P_i), differ from that of ATP hydrolysis, ATP (and water). Then, we chose to change $[\text{ATP}]$ and $[\text{ADP}]$ while keeping $[\text{ATP}] = [\text{ADP}]$ and $[\text{P}_i] = 1 \text{ mM}$. This choice keeps the driving force of ATP hydrolysis constant, which is given by the free energy change associated with the hydrolysis of a single ATP molecule

$$\Delta\mu = \Delta\mu^\circ + k_B T \ln \frac{[\text{ATP}]}{[\text{ADP}][\text{P}_i]}, \quad (2)$$

except for a slight variation in $\Delta\mu^\circ$. Here, $\Delta\mu^\circ$ is the

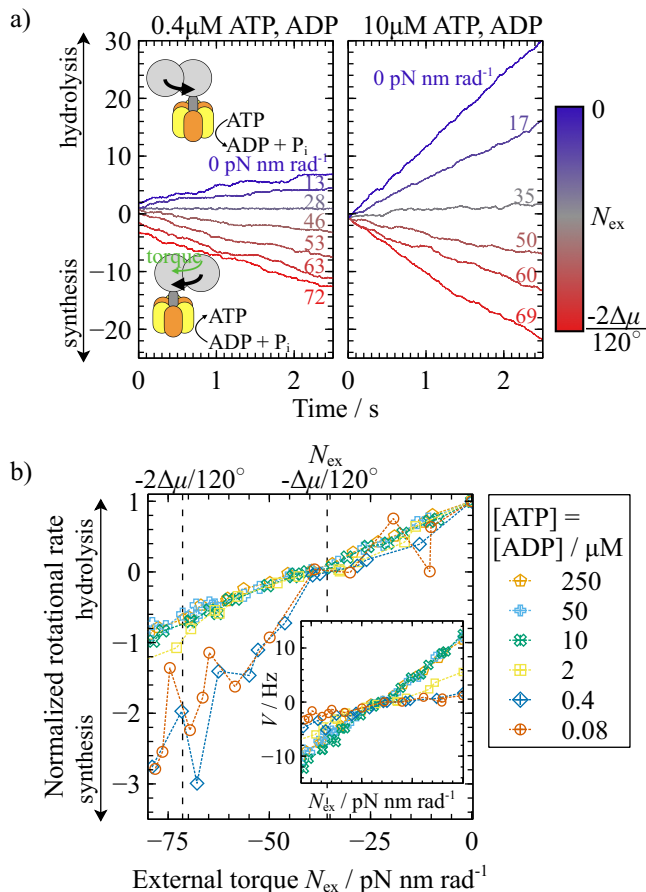


FIG. 1. a) Single-molecule trajectories in the absence and presence of external torque. The values of $[\text{ATP}] = [\text{ADP}]$ are as indicated. $[\text{P}_i] = 1 \text{ mM}$. The magnitude of the external torque is indicated on the sides of the trajectories and by the line colors. b) Examples of torque dependence of V normalized by their values at $N_{\text{ex}} = 0$. The values of $[\text{ATP}] = [\text{ADP}]$ are as indicated. $[\text{P}_i] = 1 \text{ mM}$. Data were obtained for one molecule at each concentration of ATP and ADP. Inset: Dependence of V on N_{ex} .

standard free energy change, k_B is the Boltzmann constant, and T is the ambient temperature. The values of $\Delta\mu$ were calculated as $18.2k_B T = 74.7 \text{ pN nm}$ by a method described in [22].

The dependence of the rotational rate on external torque differs between the substrate concentrations of ATP and ADP as shown in Fig. 1. The rotation and the external torque in the counterclockwise direction are defined as positive. The magnitude of the rotational rate under $N_{\text{ex}} = 63 \text{ pN nm/rad}$ is comparable with that under $N_{\text{ex}} = 0$ at $[\text{ATP}] = [\text{ADP}] = 0.4 \mu\text{M}$ (Fig. 1a, left panel), whereas the magnitude of the rotational rate under $N_{\text{ex}} = 69 \text{ pN nm/rad}$ is obviously smaller than that under $N_{\text{ex}} = 0$ at $[\text{ATP}] = [\text{ADP}] = 10 \mu\text{M}$ (Fig. 1a, right panel). Therefore, this result alone suggests that enzyme kinetics are asymmetric between ATP synthesis and hydrolysis. The difference in the dependence of

the rotational rate V on N_{ex} is clearly shown in Fig. 1b, where the rotational rates are normalized by their values at $N_{\text{ex}} = 0$, as discussed in [13]. Long pauses caused by ADP-inhibition [16, 18, 23, 24] were excluded from the calculation of V .

We examine the enzyme kinetics of F_1 in detail by fixing N_{ex} for each of ATP synthesis and hydrolysis. F_1 rotates counterclockwise (clockwise) when $N_{\text{ex}} < -\Delta\mu/120^\circ$ ($N_{\text{ex}} > -\Delta\mu/120^\circ$) (Fig. 1), indicating the tight mechanochemical coupling between the 120° rotation of F_1 and the synthesis or hydrolysis of one ATP molecule [19, 25–27]. Here, we set $N_{\text{ex}} = -2\Delta\mu/120^\circ$ for ATP synthesis and $N_{\text{ex}} = 0$ for ATP hydrolysis. This choice is equivalent to setting the magnitude of a driving force per 120° , $|N_{\text{ex}} \times 120^\circ + \Delta\mu|$, equal between ATP synthesis and hydrolysis. Because it is difficult to set $N_{\text{ex}} = -2\Delta\mu/120^\circ$ precisely, V is calculated by interpolating the rotational rate around $N_{\text{ex}} = -2\Delta\mu/120^\circ$ for ATP synthesis.

Figure 2 shows the experimental results of the dependence of the rotational rate V on the substrate concentration $[\text{S}] := [\text{ATP}] = [\text{ADP}]$ in ATP synthesis and hydrolysis. Equation (1) fits V in ATP hydrolysis, where $V_{\text{max}} = 11.8 \text{ Hz}$ and $K_m = 1.9 \mu\text{M}$, that is, F_1 's enzyme kinetics in ATP hydrolysis follow Michaelis-Menten equation. This result is qualitatively the same as that in the absence of ADP [28–39]. In ATP synthesis, V also decreases as $[\text{S}]$ decreases; however the dependence of V on $[\text{S}]$ is weaker than that in ATP hydrolysis. Equation (1) cannot describe this characteristic because the changes in V_{max} and K_m simply translate the curve of Eq. (1) on a log-log plot. The deviation from the Michaelis-Menten equation (1) can also be observed in the Lineweaver-Burk plot shown in Fig. 2b. Although a plot of V^{-1} against $[\text{S}]^{-1}$ yields a straight line when data follow Eq. (1), the experimental results for ATP synthesis were convex. These results indicate the asymmetric enzyme kinetics of F_1 between ATP synthesis and hydrolysis in the sense that their functional forms are different.

Numerical simulations.— Next, we investigated the asymmetry of the enzyme kinetics between ATP synthesis and hydrolysis based on a theoretical model. The motion of molecular motors is often described by Brownian motion in stochastically switching potentials [40]. In such a potential switching model of F_1 , the shaft angle θ follows the overdamped Langevin equation

$$\Gamma \dot{\theta} = -\frac{\partial U_n(\theta)}{\partial \theta} + N_{\text{ex}} + \sqrt{2\Gamma k_B T} \xi, \quad (3)$$

where Γ is the rotational frictional coefficient, $U_n(\theta)$ are potentials labeled by a discrete variable n , and ξ is white Gaussian noise with zero mean and unit variance. The change in the discrete variable n corresponds to the elementary reactions of F_1 , such as ATP (ADP) binding followed by ADP (ATP) release, binding and release of P_i , and the synthesis and hydrolysis of ATP at the binding

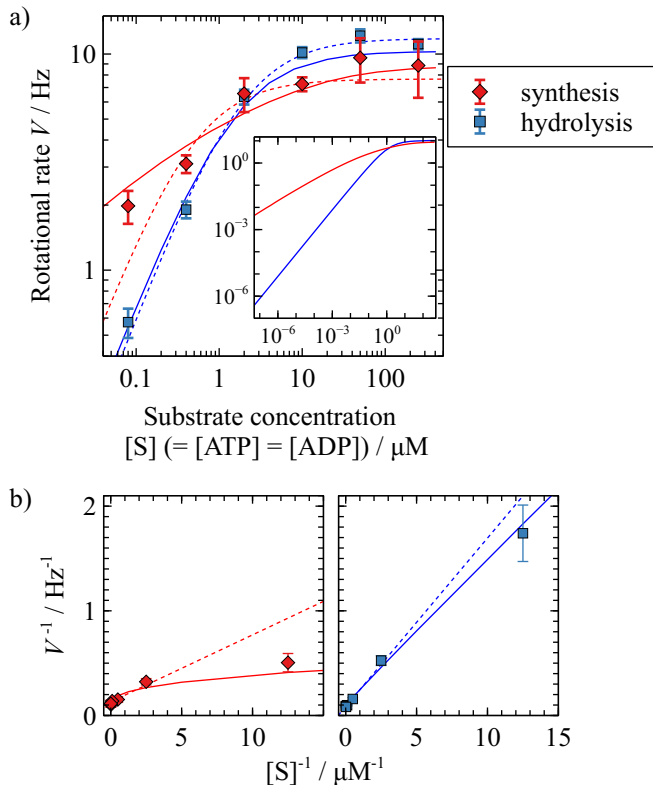


FIG. 2. Dependence of the rotational rate on substrate concentration in ATP synthesis and hydrolysis. a) Experimental and numerical results. The symbols represent the experimental results. Error bars denote standard error of the mean. Each data point is the average of 8-9 molecules. The dashed curves are fitted to the experimental results using Eq. (1). The solid curves are the numerical results obtained from the TASAM. The values of parameters set by hand are $k = 15k_B T / \text{rad}^2$, $\tilde{\Delta}\mu = 2.6k_B T$, and $\lambda = 25 / \mu\text{M}\cdot\text{s}$. Inset: Numerical results for a wide range of $[S]$, part of which is experimentally inaccessible. b) Lineweaver-Burk plot. The symbols represent the experimental results. Error bars denote standard error of the mean. The dashed lines represent $V^{-1} = V_{\text{max}}^{-1}(K_m[S]^{-1} + 1)$. The solid curves correspond to the numerical results shown in a).

sites. Here, we considered only ATP binding, followed by ADP release and its reverse reaction, as the others occur rapidly under our experimental conditions [29]. These binding events increase and decrease n by one with rates $R_n^+(\theta)$ and $R_n^-(\theta)$, respectively. The totally asymmetric allosteric model (TASAM) [13] is a potential switching model where $R_n^+(\theta)$ and $R_n^-(\theta)$ are set as

$$\begin{aligned} R_n^+(\theta) &= W, \\ R_{n+1}^-(\theta) &= W \exp\left[-\frac{U_n(\theta) - U_{n+1}(\theta) + \Delta\mu}{k_B T}\right], \end{aligned} \quad (4)$$

where W is assumed to be proportional to $[S]$ as $W = \lambda[S]$, as it characterizes the rates of these binding events. The angular dependence of $R_n^\pm(\theta)$ indicates the alloster-

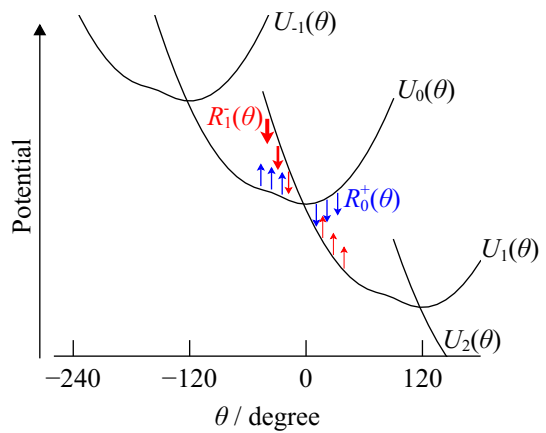


FIG. 3. Schematic of the TASAM. Solid black curves represent $U_n(\theta)$. $U_n(\theta)$ are plotted with vertical shifts $n\Delta\mu$. $R_0^+(\theta)$ and $R_1^-(\theta)$ are shown as blue and red arrows, respectively. The thicknesses of the arrows represent the magnitude of $R_0^+(\theta)$ and $R_1^-(\theta)$.

ism between the rotary shaft and the binding sites and represents how much the angle θ regulates the binding rates. The angular dependence of the ratio, $R_n^+(\theta)/R_{n+1}^-(\theta)$, imposed by local detailed balance, is entirely assigned to $R_{n+1}^-(\theta)$. In this sense, this model is referred to as totally asymmetric allosteric. It was shown in Ref. [13] that the TASAM quantitatively reproduce the experimental result of F_1 [41] (a similar argument was made in [12]). Taking into account the threefold symmetry of the $\alpha_3\beta_3$ subcomplex surrounding the rotary shaft of F_1 , a translational symmetry $U_n(\theta) = U_{n+1}(\theta + 120^\circ)$ was imposed on $U_n(\theta)$. A schematic of the TASAM is shown in Fig. 3.

We numerically solved a master equation of TASAM to obtain the steady state distribution of θ and n and evaluated V as a function of $[S]$ (See the Supplemental Material [17] for details). We used the effective potential in [13] as $U_0(\theta)$.

$$\begin{aligned} U_0(\theta) &= -k_B T \ln \left[\exp\left(-\frac{k\theta^2}{2k_B T}\right) \right. \\ &\quad \left. + \exp\left(-\frac{k(\theta + 40^\circ)^2}{2k_B T} - \tilde{\Delta}\mu\right) \right], \end{aligned} \quad (5)$$

which is a potential obtained by coarse-graining two harmonic potentials with a common spring constant k , angular displacement 40° , and height difference $\tilde{\Delta}\mu$. We adjusted the values of k , $\tilde{\Delta}\mu$, and λ by hand to align the numerical results of V with the experimental results of V . We set $\Gamma = 0.1k_B T\text{s}/\text{rad}^2 = 0.4\text{pN}\cdot\text{nm}\cdot\text{s}/\text{rad}^2$ from experimentally obtained values of diffusion coefficients, and $T = 298\text{K}$. The numerical results reproduced two characteristics of the experimental results: the weak dependence of V on $[S]$ in ATP synthesis, which Eq. (1) can-

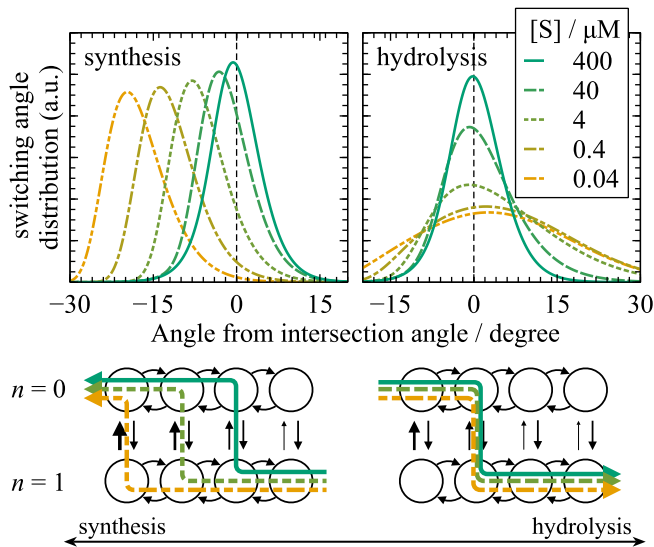


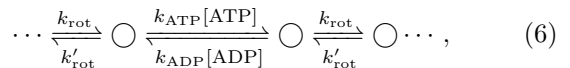
FIG. 4. Switching angle distribution with a schematic of the path in a space of θ and n in ATP synthesis and hydrolysis. The switching angle distribution is given as a difference between the angular distribution of the forward switching from $n = 0$ to $n = 1$ and that of the backward switching from $n = 1$ to $n = 0$. The heights of the switching angle distributions are normalized. The origin of the horizontal axis is set at an intersection point of potentials. The parameters in the numerical simulations are the same as those shown in Fig. 2. In the schematic, the angle is represented as a discrete variable. The thicknesses of the vertical arrows represent the magnitude of $R_0^+(\theta)$ and $R_1^-(\theta)$.

not describe, and the enzyme kinetics following Eq. (1) in ATP hydrolysis (Fig. 2a). Therefore, the theoretical model supports the experimental results that the enzyme kinetics of F_1 deviate from Eq. (1) in ATP synthesis, whereas it follows Eq. (1) in ATP hydrolysis.

We focused on the switching angle distribution to elucidate the mechanism underlying the asymmetry in the enzyme kinetics of F_1 between ATP synthesis and hydrolysis (Fig. 4). It was shown that the dependence of the switching angle distribution on $[S]$ is asymmetric between ATP synthesis and hydrolysis [13]. We numerically calculated the switching angle distribution at several concentrations $[S]$ using the steady state distribution of θ and n . The peak position of the switching angle distribution is kept almost constant around the intersection point of potentials, where $U_n(\theta) - U_{n+1}(\theta) + \Delta\mu = 0$, irrespective of $[S]$ in ATP hydrolysis, but shifts in the negative direction in ATP synthesis as $[S]$ decreases as discussed in Ref. [13]. The switching around the intersection point in ATP hydrolysis was experimentally observed [42]. The peak shift in ATP synthesis suggests that a path in a space of θ and n changes with $[S]$ (bottom panel in Fig. 4). At high $[S]$, ADP binds quickly around the intersection

point, and then the shaft rotates. In contrast, at low $[S]$, the shaft rotates beyond the intersection point, and then ATP binds. That is, the path where substrate binding is slow is bypassed. In other words, the uphill rotation of F_1 caused by thermal fluctuations partially compensates for the decrease in the substrate binding rate. This compensation does not occur in ATP hydrolysis, because the binding rate of ATP, $R_n^+(\theta)$, does not increase, even if F_1 climbs up the potential slope [Eq. (4)].

This bypass mechanism causes the asymmetry in the enzyme kinetics as follows. As seen in Fig. 2a, the dependence of V on $[S]$ in ATP synthesis is weaker than $V \propto [S]$, even at low $[S]$. V is proportional to $[S]$ when the binding of the substrate is rate-limiting; therefore, this result indicates that the bypass mechanism prevents the binding of ADP from becoming a rate-limiting step. As a result, the enzyme kinetics deviated from Eq. (1). In contrast, the peak position remains almost constant in ATP hydrolysis. This means that the rates of ATP binding followed by ADP release and its reverse reaction, written as $k_{\text{ATP}}[\text{ATP}]$ and $k_{\text{ADP}}[\text{ADP}]$, respectively, are independent of θ . Here, k_{ATP} and k_{ADP} are bimolecular rate constants. As a result, the reaction can be described using a sequential scheme



and its enzyme kinetics follows Eq. (1). Here, k_{rot} and k'_{rot} are rate constants corresponding to $\pm 120^\circ$ rotation.

We investigated whether the asymmetric allosterism represented by Eq. (4) is essential to the asymmetric enzyme kinetics we observed in the experiments. Since asymmetric potential profiles could also induce asymmetric enzyme kinetics, we compared two cases: asymmetric allosterism with symmetric potentials and symmetric allosterism with asymmetric potentials. Symmetric rates

$$R_n^+(\theta) = W \exp \left[\frac{U_n(\theta) - U_{n+1}(\theta) + \Delta\mu}{2k_{\text{B}}T} \right], \quad (7)$$

$$R_{n+1}^-(\theta) = W \exp \left[-\frac{U_n(\theta) - U_{n+1}(\theta) + \Delta\mu}{2k_{\text{B}}T} \right]$$

were used for the symmetric allosterism. Asymmetric potentials were constructed by concatenating harmonic potentials with different spring constants κ and κ' ,

$$U_0(\theta) = \begin{cases} \frac{1}{2}\kappa\theta^2 & \theta \geq 0, \\ \frac{1}{2}\kappa'\theta^2 & \theta < 0, \end{cases} \quad (8)$$

and controlled its asymmetry through the ratio of κ and κ' . The enzyme kinetics for these cases were numerically evaluated (Fig. 5a). The asymmetric allosterism with symmetric potentials induced asymmetric enzyme kinetics between ATP synthesis and hydrolysis, qualitatively reproducing those of the TASAM (Fig. 2a). The

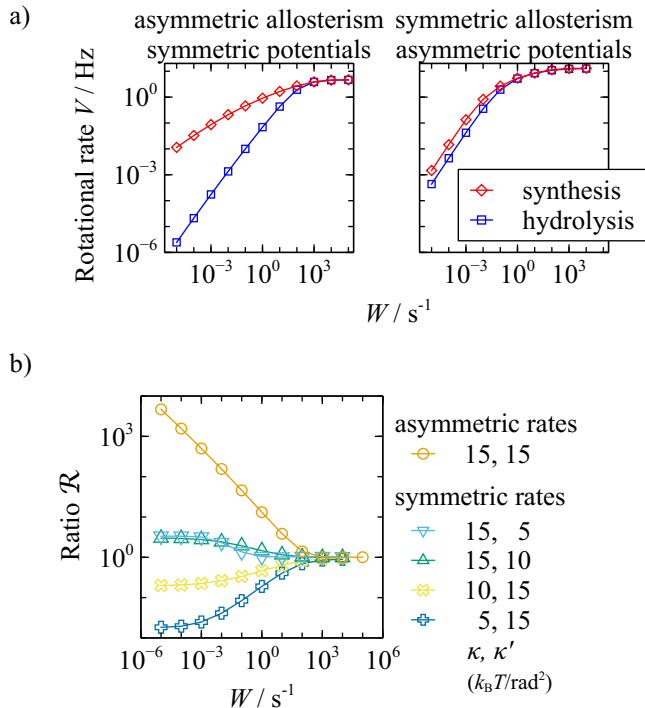


FIG. 5. Comparison between asymmetric allostery with symmetric potentials, and symmetric allostery with asymmetric potentials. a) Dependence of V on W in ATP synthesis and hydrolysis. $\kappa = \kappa' = 15k_B T / \text{rad}^2$ for symmetric potentials, and $\kappa = 15k_B T / \text{rad}^2$, $\kappa' = 5k_B T / \text{rad}^2$ for asymmetric potentials. b) Dependence of ratios of V in ATP synthesis to V in ATP hydrolysis, \mathcal{R} , on W .

enzyme kinetics for symmetric allostery with asymmetric potentials were similar to the Michaelis-Menten kinetics [Eq. (1)] in that V was proportional to W at small W .

The asymmetry of the enzyme kinetics can be measured by the ratio of V in ATP synthesis and hydrolysis, \mathcal{R} (Fig. 5b). With asymmetric allostery, \mathcal{R} continued to increase as W decreases, indicating the deviation of ATP synthesis from the Michaelis-Menten kinetics. In contrast, with symmetric allostery, \mathcal{R} converge as W decreases even with significant asymmetry in κ and κ' , reflecting the fact that both ATP hydrolysis and synthesis approximately follow Michaelis-Menten kinetics. Thus, the asymmetric allostery is essential for the asymmetric enzyme kinetics.

Concluding remarks.— In this Letter, we reveal that the enzyme kinetics of F_1 are asymmetric between ATP synthesis and hydrolysis. We demonstrate that the asymmetry in the angular dependence of the substrate binding rates, which is a characteristic of the TASAM, leads to asymmetric enzyme kinetics by a novel bypass mechanism.

Before concluding this Letter, we discuss the physical significance of our results. We observed that

ATP synthesis was faster than ATP hydrolysis at low $[ATP]$ and $[ADP]$ under our experimental conditions. One might be tempted to conclude that the asymmetric allostery of F_1 was developed by evolution to sustain the rate of ATP synthesis while suppressing futile ATP consumption, similar to ADP-inhibition, ϵ subunit, and IF_1 . However, in experiments with F_oF_1 reconstituted into liposomes, the enzyme kinetics of ATP synthesis were reported to follow the Michaelis-Menten kinetics [43–45]. Because there are various differences in experimental conditions, e.g. ratio of $[ATP]$ to $[ADP]$, $[P_i]$, N_{ex} , and Γ , which could alter the rate-limiting steps of the enzyme kinetics. Hence, it is not straightforward to compare their experimental results with ours. Experiments with extensively controlled conditions may bridge such gap and pave the way for elucidating the design principles of F_1 .

This work was supported by JSPS KAKENHI Grant Numbers JP18H05427, JP19H01864, and JP23H01136, and JST ERATO Grant Number JPMJER2302.

* toyabe@tohoku.ac.jp

- [1] B. Alberts, R. Heald, K. Hopkin, A. D. Johnson, D. O. Morgan, K. K. Roberts, and P. Walter, *Essential cell biology*, 6th ed. (W.W. Norton & Company, 2023).
- [2] J. P. Abrahams, A. G. W. Leslie, R. Lutter, and J. E. Walker, *Nature* **370**, 621 (1994).
- [3] R. E. Ebel and H. A. Lardy, *J. Biol. Chem.* **250**, 191 (1975).
- [4] S. Schuster, R. Ebel, and H. Lardy, *J. Biol. Chem.* **250**, 7848 (1975).
- [5] B. Chernyak, V. Chernyak, T. Gladysheva, Z. Kozhanova, and I. Kozlov, *Biochim. Biophys. Acta, Bioenerg.* **635**, 552 (1981).
- [6] R. L. Cross, C. Grubmeyer, and H. S. Penefsky, *J. Biol. Chem.* **257**, 12101 (1982).
- [7] M. J. Gresser, J. A. Myers, and P. D. Boyer, *J. Biol. Chem.* **257**, 12030 (1982).
- [8] S. Y. Wong, A. Matsuno-Yagi, and Y. Hatefi, *Biochemistry* **23**, 5004 (1984).
- [9] O. A. Roveri and N. B. Calcaterra, *FEBS Lett.* **192**, 123 (1985).
- [10] J. Jault and W. Allison, *J. Biol. Chem.* **268**, 1558 (1993).
- [11] A. S. Lapashina and B. A. Feniouk, *Biochemistry (Moscow)* **83**, 1141 (2018).
- [12] E. Zimmermann and U. Seifert, *New J. Phys.* **14**, 103023 (2012).
- [13] K. Kawaguchi, S.-i. Sasa, and T. Sagawa, *Biophys. J.* **106**, 2450 (2014).
- [14] M. Washizu, Y. Kurahashi, H. Iochi, O. Kurosawa, S. Aizawa, S. Kudo, Y. Magariyama, and H. Hotani, *IEEE Trans. Ind. Appl.* **29**, 286 (1993).
- [15] T. Watanabe-Nakayama, S. Toyabe, S. Kudo, S. Sugiyama, M. Yoshida, and E. Muneyuki, *Biochem. Biophys. Res. Commun.* **366**, 951 (2008).
- [16] Y. Nakayama and S. Toyabe, *Phys. Rev. Lett.* **126**, 208101 (2021).
- [17] See Supplemental Material at [URL] for materials and

methods.

- [18] H. Noji, R. Yasuda, M. Yoshida, and K. Kinosita, *Nature* **386**, 299 (1997).
- [19] S. Toyabe, T. Watanabe-Nakayama, T. Okamoto, S. Kudo, and E. Muneyuki, *PNAS* **108**, 17951 (2011).
- [20] H. Itoh, A. Takahashi, K. Adachi, H. Noji, R. Yasuda, M. Yoshida, and K. Kinosita, *Nature* **427**, 465 (2004).
- [21] Y. Rondelez, G. Tresset, T. Nakashima, Y. Kato-Yamada, H. Fujita, S. Takeuchi, and H. Noji, *Nature* **433**, 773 (2005).
- [22] K. Krab and J. van Wezel, *Biochim. Biophys. Acta, Bioenerg.* **1098**, 172 (1992).
- [23] Y. Hirono-Hara, H. Noji, M. Nishiura, E. Muneyuki, K. Y. Hara, R. Yasuda, K. Kinosita, and M. Yoshida, *PNAS* **98**, 13649 (2001).
- [24] Y. Hirono-Hara, K. Ishizuka, K. Kinosita, M. Yoshida, and H. Noji, *PNAS* **102**, 4288 (2005).
- [25] S. Toyabe and E. Muneyuki, *New J. Phys.* **17**, 015008 (2015).
- [26] E.-i. Saita, T. Suzuki, K. Kinosita, and M. Yoshida, *PNAS* **112**, 9626 (2015).
- [27] N. Soga, K. Kimura, K. Kinosita, M. Yoshida, and T. Suzuki, *PNAS* **114**, 4960 (2017).
- [28] R. Yasuda, H. Noji, K. Kinosita, and M. Yoshida, *Cell* **93**, 1117 (1998).
- [29] R. Yasuda, H. Noji, M. Yoshida, K. Kinosita, and H. Itoh, *Nature* **410**, 898 (2001).
- [30] H. Noji, D. Bald, R. Yasuda, H. Itoh, M. Yoshida, and K. Kinosita, *J. Biol. Chem.* **276**, 25480 (2001).
- [31] S. Bandyopadhyay, C. R. Valder, H. G. Huynh, H. Ren, and W. S. Allison, *Biochemistry* **41**, 14421 (2002).
- [32] N. Sakaki, R. Shimo-Kon, K. Adachi, H. Itoh, S. Furuike, E. Muneyuki, M. Yoshida, and K. Kinosita, *Biophys. J.* **88**, 2047 (2005).
- [33] K. Adachi, K. Oiwa, T. Nishizaka, S. Furuike, H. Noji, H. Itoh, M. Yoshida, and K. Kinosita Jr., *Cell* **130**, 309 (2007).
- [34] R. Watanabe, R. Iino, K. Shimabukuro, M. Yoshida, and H. Noji, *EMBO Rep.* **9**, 84 (2008).
- [35] S. Furuike, K. Adachi, N. Sakaki, R. Shimo-Kon, H. Itoh, E. Muneyuki, M. Yoshida, and K. Kinosita Jr., *Biophys. J.* **95**, 761 (2008).
- [36] M. Tsumuraya, S. Furuike, K. Adachi, K. Kinosita, and M. Yoshida, *FEBS Lett.* **583**, 1121 (2009).
- [37] D. Okuno, M. Nishiyama, and H. Noji, *Biophys. J.* **105**, 1635 (2013).
- [38] A. Yukawa, R. Iino, R. Watanabe, S. Hayashi, and H. Noji, *Biochemistry* **54**, 472 (2015).
- [39] R. Watanabe, M. Genda, Y. Kato-Yamada, and H. Noji, *Biophys. J.* **114**, 178 (2018).
- [40] T. Elston, H. Wang, and G. Oster, *Nature* **391**, 510 (1998).
- [41] S. Toyabe, T. Okamoto, T. Watanabe-Nakayama, H. Taketani, S. Kudo, and E. Muneyuki, *Phys. Rev. Lett.* **104**, 10.1103/PhysRevLett.104.198103 (2010).
- [42] S. Toyabe, H. Ueno, and E. Muneyuki, *EPL* **97**, 40004 (2012).
- [43] D. Bald, T. Amano, E. Muneyuki, B. Pitard, J.-L. Rigaud, J. Kruip, T. Hisabori, M. Yoshida, and M. Shibata, *J. Biol. Chem.* **273**, 865 (1998).
- [44] R. Iino, R. Hasegawa, K. V. Tabata, and H. Noji, *J. Biol. Chem.* **284**, 17457 (2009).
- [45] N. Soga, K. Kinosita, M. Yoshida, and T. Suzuki, *FEBS J.* **278**, 2647 (2011).

Supplemental Material for “Bypass mechanism of F₁-ATPase for asymmetric enzyme kinetics”

Yohei Nakayama¹ and Shoichi Toyabe¹

¹*Department of Applied Physics, Graduate School of Engineering,
Tohoku University, Aoba 6-6-05, Sendai 980-8579, Japan*

I. MATERIALS AND METHODS

A. Preparation of F₁

$\alpha_3\beta_3\gamma$ subcomplexes of F₁ derived from a thermophilic *Bacillus* PS3 with mutations for the rotation assay (His₆- α C193S/W463F, His₁₀- β , and γ S107C/I210C) [1] were expressed and purified in the same way as [2], except that the treatment with (\pm)-dithiothreitol before flash freezing was omitted.

B. Ni²⁺-NTA modification of cover glasses

In our single-molecule experiments, F₁ molecules were adhered to a cover glass modified by Ni²⁺-NTA. The Ni²⁺-NTA glass was prepared as follows. Cover glasses (24 × 36mm² or 24 × 32mm², thickness No. 1; Matsunami) were washed with ultrapure water three times and immersed in 10 M potassium hydroxide solution overnight. The glasses were washed with RO water five times and ultrapure water one time, and immersed in a 1:1 mixture of ethanol and ultrapure water containing 2 % v/v (3-Mercaptopropyl)trimethoxysilane (purchased from TCI, Japan) and 0.06 % v/v acetic acid for 120 min at 60 °C. They were washed with ultrapure water three times, and baked at 120 °C for 60 min. They were immersed in 50 mM phosphate buffer (pH 6.7) containing 1 mM (\pm)-dithiothreitol and 2 mM ethylenediaminetetraacetic acid for 90 min. They were washed with RO water five times and ultrapure water one time, and reacted with 1.8 mg/ml Maleimido-C₃-NTA (purchased from Dojindo, Japan) in 100 mM phosphate buffer (pH 6.7) for 60 min. The glasses were immersed in 50 mM nickel sulfate solution for 30 min, and washed with RO water five times and ultrapure water one time, before using them for single-molecule experiments.

C. Single-molecule experiments

The experimental setup is essentially the same as that in the previous study [2]. An observation chamber consisted of a Ni²⁺-NTA modified cover glass and a slide with quadrupolar electrodes. The cover glass and the slide were separated by double-sided adhesive tape (10 μ m thickness; Teraoka, 7070W) with silicone grease (Shin-Etsu Chemical, Japan) on a surface. The solution of F₁ was diluted with 50 mM MOPS buffer (pH 6.7) containing 5 mg/ml bovine serum albumin, 50 mM potassium chloride, and 1 mM magnesium chloride (buffer II) to a final concentration of 1 nM. The chamber was filled with the solution, and incubated for 10 min to immobilize F₁ molecules on the surfaces. The bovine serum albumin was added as the blocking agent. The chamber was washed with buffer II, and streptavidin-coated polystyrene particles (diameter = 276 nm, Thermo Fisher Scientific) diluted with buffer II was infused into it. Azide contained in the solution of polystyrene particle was removed in advance by repeating centrifugation, exchange of supernatant, and re-dispersion six times. After a 30 min incubation, the solution in the chamber was exchanged with 5 mM MOPS and 1 mM phosphate buffer containing 1 mM magnesium chloride, and indicated amount of MgATP and MgADP (pH 7.0).

Rotation of the γ -shaft was probed by dimeric polystyrene particles attached to the biotinylated γ -shaft. The observation was performed on a bright-field upright microscope (Olympus, Japan) with a 100× objective (NA1.40), high-intensity LED (623 nm, 4.8 W, Thorlabs, NJ) for illumination, a high-speed camera (Basler, Germany) at 4,000 Hz, and a laboratory-made capturing software developed on LabVIEW (National Instruments, TX). The angular position of the dimeric probe was analyzed by an algorithm based on a principal component analysis of the probe image.

We used a laboratory-made autofocus system to keep the probe in focus with a stepping motor (Oriental motor, Japan) rotating a focus knob.

We observed 8 molecules for [ATP] = [ADP] = 0.08 μ M, 9 molecules for [ATP] = [ADP] = 0.4 μ M, 8 molecules for [ATP] = [ADP] = 2 μ M, 8 molecules for [ATP] = [ADP] = 10 μ M, 9 molecules for [ATP] = [ADP] = 50 μ M, and 9 molecules for [ATP] = [ADP] = 250 μ M.

We applied an external torque on the probe attached to F₁ by using electrorotation method as described in [2]

D. Numerical calculation

We first obtained the probability distribution of θ and n at the steady state $P^{\text{st}}(\theta, n)$ by numerically solving a master equation of the TASAM. The master equation of the TASAM is written as

$$\begin{aligned} \frac{\partial P_t(\theta, n)}{\partial t} = & -\frac{\partial}{\partial \theta} \left[\frac{1}{\Gamma} \left(N_{\text{ex}} - \frac{\partial U_n(\theta)}{\partial \theta} \right) P_t(\theta, n) - \frac{k_B T}{\Gamma} \frac{\partial P_t(\theta, n)}{\partial \theta} \right] \\ & + R_{n-1}^+(\theta) P_t(\theta, n-1) + R_{n+1}^-(\theta) P_t(\theta, n+1) - [R_n^+(\theta) + R_n^-(\theta)] P_t(\theta, n). \end{aligned} \quad (\text{S1})$$

Since $P^{\text{st}}(\theta, n)$ satisfies translational symmetry $P^{\text{st}}(\theta, n) = P^{\text{st}}(\theta + 120^\circ, n+1)$, we simplified Eq. (S1) by imposing the same translational symmetry on $P_t(\theta, n)$ as

$$\begin{aligned} \frac{\partial P_t(\theta, 0)}{\partial t} = & -\frac{\partial}{\partial \theta} \left[\frac{1}{\Gamma} \left(N_{\text{ex}} - \frac{\partial U_0(\theta)}{\partial \theta} \right) P_t(\theta, 0) - \frac{k_B T}{\Gamma} \frac{\partial P_t(\theta, 0)}{\partial \theta} \right] \\ & + R_0^+(\theta + 120^\circ) P_t(\theta + 120^\circ, 0) + R_0^-(\theta - 120^\circ) P_t(\theta - 120^\circ, 0) - [R_0^+(\theta) + R_0^-(\theta)] P_t(\theta, 0). \end{aligned} \quad (\text{S2})$$

We introduced reflecting boundaries at θ_b^+ and θ_b^- , and discretized angular space with an interval $\Delta\theta = 0.5^\circ$. Then, we obtained $P^{\text{st}}(\theta, 0)$ by evolving $P_t(\theta, 0)$ using Euler method with the temporal interval $\Delta t = 10^{-8}$ s or 10^{-9} s.

The rotational rate V was evaluated from $P^{\text{st}}(\theta, 0)$ as follows. V is related with a probability current in θ -direction at the steady state

$$J_\theta^{\text{st}} = \sum_{n=-\infty}^{\infty} \left[\frac{1}{\Gamma} \left(N_{\text{ex}} - \frac{\partial U_n(\theta)}{\partial \theta} \right) P^{\text{st}}(\theta, n) - \frac{k_B T}{\Gamma} \frac{\partial P^{\text{st}}(\theta, n)}{\partial \theta} \right], \quad (\text{S3})$$

as $V = J_\theta^{\text{st}}/3$. Then, we evaluated J_θ^{st} by rewriting Eq. (S3) as

$$J_\theta^{\text{st}} = \sum_{n=-\infty}^{\infty} \left[\frac{1}{\Gamma} \left(N_{\text{ex}} - \frac{\partial U_0(\theta - n \cdot 120^\circ)}{\partial \theta} \right) P^{\text{st}}(\theta - n \cdot 120^\circ, 0) - \frac{k_B T}{\Gamma} \frac{\partial P^{\text{st}}(\theta - n \cdot 120^\circ, 0)}{\partial \theta} \right], \quad (\text{S4})$$

and converted it to V .

The switching angle distribution is defined as $\Lambda_n(\theta) = R_n^+(\theta) P^{\text{st}}(\theta, n) - R_{n+1}^-(\theta) P^{\text{st}}(\theta, n+1)$. We evaluated $\Lambda_0(\theta)$ as

$$\Lambda_0(\theta) = R_0^+(\theta) P^{\text{st}}(\theta, 0) - R_0^-(\theta - 120^\circ) P^{\text{st}}(\theta - 120^\circ, 0). \quad (\text{S5})$$

$\Lambda_n(\theta)$ may be obtained as $\Lambda_n(\theta) = \Lambda_0(\theta - n \cdot 120^\circ)$ from the translational symmetry.

-
- [1] Y. Rondelez, G. Tresset, T. Nakashima, Y. Kato-Yamada, H. Fujita, S. Takeuchi, and H. Noji, *Nature* **433**, 773 (2005).
 [2] Y. Nakayama and S. Toyabe, *Phys. Rev. Lett.* **126**, 208101 (2021).